

# Shallow-KAN Based Solution of Moving Boundary PDEs

Tarus Pande<sup>a</sup>, V M S K Minnikanti<sup>a</sup>, Shyamprasad Karagadde<sup>a,b,\*</sup>

<sup>a</sup> Department of Mechanical Engineering

<sup>b</sup> Centre for Machine Intelligence and Data Science

Indian Institute of Technology Bombay, Mumbai 400076, India

\* Corresponding Author: s.karagadde@iitb.ac.in

## Abstract

Kolmogorov–Arnold Networks (KANs) require significantly smaller architectures compared to multilayer perceptron (MLP)-based approaches, while retaining expressive power through spline-based activations. We propose a shallow KAN framework that directly approximates the temperature distribution  $T(\mathbf{x}, t)$  and the moving interface  $\Gamma(t)$ , enforcing the governing PDEs, phase equilibrium, and Stefan condition through physics-informed residuals. To enhance accuracy, we employ interface-focused collocation resampling. Numerical experiments in one and two dimensions show that the framework achieves accurate reconstructions of both temperature fields and interface dynamics, highlighting the potential of KANs as a compact and efficient alternative for moving boundary PDEs. First, we validate the model with semi-infinite analytical solutions. Subsequently, the model is extended to 2D using a level-set based formulation for interface propagation, which is solved within the KAN framework. This work demonstrates that KANs are capable of solving complex moving boundary problems without the need for measurement data.

## 1 Introduction

Phase-change phenomena is ubiquitous and has applications in material processing [1–3], energy systems [4], biomedical [5, 6], geophysical [7]. Phase-change problems such as melting and solidification are commonly formulated as moving-boundary (Stefan-type) problems, where coupled transport PDEs determine the evolution of an interface separating phases [1, 8]. The interface (boundary dividing different phases) evolution is commonly modelled using a sharp [9, 10] or diffuse [11, 12] or hybrid-approaches [13]. For Stefan-type problems, stability and accuracy are tightly linked to how well the interface conditions and latent-heat balance are enforced; small temperature errors can induce large interface-location errors over time, motivating alternative space–time formulations beyond conventional discretisations [14–16].

Physics-Informed Neural Networks (PINNs) [17] approximate the solution with a neural network trained by a loss composed of governing physics and are demonstrated to solve both forward and inverse problems [18–20]. Despite their appeal, PINNs face several challenges when extended to solve moving boundary problems. Firstly, they often have to incorporate measurement data to stabilize training, particularly in nonlinear heat transfer and two-phase Stefan problems [18]. Secondly, limited by spectral bias, standard PINNs struggle to resolve high-frequency variations [21, 22], which may affect the accuracy of gradients and sharp-boundary conditions on interfaces. Consequently, solving moving boundary PDEs generally requires deeper network architectures, which increases training cost and hampers the interpretability of the solution [23]. In a recent study [24] investigated the use of PINN for phase transition problems, with adaptive weighting scheme and residual balancing and require substantial optimization effort and tuning. Another study by Mullins et al. [25] used MLP-type architecture for level-set equation to handle interfacial dynamics and demonstrated comparable performance similar to conventional

techniques but may need careful tuning of weights and deep networks may demand very high sampling to extend it to coupled heat-transfer/stefan-type interface problems.

In contrast to MLP based architectures, the recently proposed Kolmogorov-Arnold Networks (KANs) [26], grounded in the Kolmogorov-Arnold representation theorem [27, 28], have better interpretability and accuracy with shallower networks. They incorporate nonlinearity directly into learnable basis functions on the network edges rather than relying on fixed node activations, KANs with shallower networks matched comparable accuracy of standard MLP PINNs [26]. Recent studies have demonstrated that KANs effectively mitigate the spectral bias observed in standard MLP-based PINNs, enabling the efficient capture of fine-scale features and sharp gradients [29]. In this work, we propose a shallow KAN framework that approximates the temperature distribution and the moving interface by enforcing the governing PDEs, phase equilibrium (dirichlet condition of interface), and Stefan condition through physics-informed residuals. Interface capture is handled using Level Set method [30] adopted to KAN architecture.

To enhance the accuracy near the moving boundary, we employ interface-focused collocation resampling. We validate the framework on benchmark 1D and 2D Stefan problems with available reference solutions (closed-form or high-fidelity numerical), reporting errors in both the temperature field and the inferred interface location, without using measurement data.

## 2 Problem Statement & Methodology

The Stefan problem is a classical free-boundary problem modeling phase-change processes such as melting and solidification [31, 32]. Let  $\Omega \subset \mathbb{R}^3$  denote the spatial domain, initially partitioned into a liquid region  $\Omega_\ell(0)$  and a solid region  $\Omega_s(0)$ , separated by an interface  $\Gamma(0)$ . The objective is to determine the temperature fields  $u_\ell(\mathbf{x}, t)$  and  $u_s(\mathbf{x}, t)$  in  $\Omega_\ell(t)$  and  $\Omega_s(t)$ , respectively, together with the evolution of the moving interface  $\Gamma(t)$ .

Heat conduction in each phase is governed by

$$\partial_t u_\ell = \alpha_\ell \nabla^2 u_\ell, \quad \mathbf{x} \in \Omega_\ell(t), \quad (1)$$

$$\partial_t u_s = \alpha_s \nabla^2 u_s, \quad \mathbf{x} \in \Omega_s(t), \quad (2)$$

where  $\alpha_i = k_i / (\rho_i c_{p,i})$  denotes the thermal diffusivity of phase  $i \in \{\ell, s\}$ .

At the interface  $\Gamma(t)$ , the temperature satisfies the equilibrium condition

$$u_\ell = u_s = T_m, \quad \mathbf{x} \in \Gamma(t), \quad (3)$$

and the interface motion is governed by the Stefan condition [31, 32]

$$\rho_s L v_n = k_s \nabla u_s \cdot \mathbf{n} - k_\ell \nabla u_\ell \cdot \mathbf{n}, \quad \mathbf{x} \in \Gamma(t), \quad (4)$$

where  $\mathbf{n}$  is the unit normal pointing into the liquid phase and  $v_n$  is the normal interface velocity.

At  $t = 0$ , the temperature field is prescribed as

$$u(\mathbf{x}, 0) = \begin{cases} u_s^0(\mathbf{x}), & \mathbf{x} \in \Omega_s(0), \\ u_\ell^0(\mathbf{x}), & \mathbf{x} \in \Omega_\ell(0), \end{cases} \quad (5)$$

and appropriate boundary conditions are imposed on the external boundary  $\partial\Omega$ .

In one-dimensional phase-change problems, the solid–liquid interface can be described explicitly by a single-valued function of time. In contrast, in multi-dimensional settings the interface may undergo topological changes and cannot, in general, be represented as a single-valued graph. To handle such geometrical complexity, we adopt the *level set method*, in which the moving interface is represented implicitly by a smooth scalar field  $\phi(\mathbf{x}, t)$  defined over the spatial domain  $\mathbf{x} \in \mathbb{R}^n$ , such that

$$\Gamma(t) = \{\mathbf{x} \in \mathbb{R}^n : \phi(\mathbf{x}, t) = 0\}, \quad (6)$$

where  $\Gamma(t)$  denotes the moving phase boundary. The sign of  $\phi$  distinguishes the two regions:

$$\Omega_s(t) = \{\mathbf{x} : \phi(\mathbf{x}, t) < 0\}, \quad (7)$$

$$\Omega_\ell(t) = \{\mathbf{x} : \phi(\mathbf{x}, t) > 0\}. \quad (8)$$

The unit normal vector pointing from solid to liquid is given by

$$\mathbf{n} = \frac{\nabla \phi}{\|\nabla \phi\|}, \quad (9)$$

and the evolution of  $\phi$  satisfies the level set advection equation,

$$\phi_t + v_n \|\nabla \phi\| = 0, \quad (10)$$

where  $v_n$  is the normal velocity of the interface.

In the Stefan problem, this velocity is determined by the balance of heat fluxes across the interface 4. The temperature continuity at the interface is imposed via equation 3.

This level set framework provides a unified and dimension-independent representation for the moving interface, enabling straightforward extension to both two- and three-dimensional Stefan problems.

We now generalize the KAN-based solution framework for the  $n$ -dimensional two-phase Stefan problem. The model employs three KAN subnetworks to represent the unknown fields:

$$(u_s(\mathbf{x}, t), u_\ell(\mathbf{x}, t), \phi(\mathbf{x}, t)),$$

where  $u_s$  and  $u_\ell$  are the temperature fields in the solid and liquid phases, and  $\phi$  is the level set function defining the moving interface.

The overall loss function  $\mathcal{L}$  is composed of multiple residual terms that enforce the PDEs, interface conditions, and physical constraints:

$$\mathcal{L} = \mathcal{L}_{\text{PDE},s} + \mathcal{L}_{\text{PDE},\ell} + \mathcal{L}_{\text{Interface}} + \mathcal{L}_{\text{Advection}} + \mathcal{L}_{\text{Eikonal}} + \mathcal{L}_{\text{BC}} + \mathcal{L}_{\text{IC}}. \quad (11)$$

The diffusion equations in the solid and liquid phases are enforced through smoothly masked PDE residuals,

$$\mathcal{L}_{\text{PDE},s} = \|(u_{s,t} - \alpha_s \nabla^2 u_s) H_s(\phi(\mathbf{x}, t))\|^2, \quad (12)$$

$$\mathcal{L}_{\text{PDE},\ell} = \|(u_{\ell,t} - \alpha_\ell \nabla^2 u_\ell) H_\ell(\phi(\mathbf{x}, t))\|^2, \quad (13)$$

where  $H_s$  and  $H_\ell$  denote smooth approximations of the characteristic functions of the solid and liquid regions, respectively. These masks are defined using a smoothed Heaviside function,

$$H_\ell(\phi) = \sigma(\beta\phi), \quad (14)$$

$$H_s(\phi) = 1 - \sigma(\beta\phi), \quad (15)$$

with  $\sigma(z) = (1 + e^{-z})^{-1}$  denoting the sigmoid function. Since  $\phi(\mathbf{x}, t)$  is the signed distance function from the interface, choosing a large value of  $\beta$  (here  $\beta = 100$ ) yields a narrow transition zone, providing a smooth yet sharp approximation to the indicator functions of the liquid ( $\phi > 0$ ) and solid ( $\phi < 0$ ) domains.

To weakly enforce temperature continuity across the interface, we define the interface loss

$$\mathcal{L}_{\text{Interface}} = \int_{\Omega} \left[ (u_s(\mathbf{x}, t) - T_m)^2 + (u_\ell(\mathbf{x}, t) - T_m)^2 \right] w_\Gamma(\phi(\mathbf{x}, t)) d\mathbf{x}, \quad (16)$$

where the interface weighting function is chosen as a Gaussian centered at the zero level set,

$$w_\Gamma(\phi) = \exp\left(-\frac{\phi^2}{\varepsilon_\Gamma^2}\right). \quad (17)$$

The Gaussian weighting localizes the loss to a narrow band around the moving interface  $\Gamma(t) = \{\mathbf{x} : \phi(\mathbf{x}, t) = 0\}$ , providing a smooth and differentiable approximation to the sharp interface temperature continuity condition.

The level-set function  $\phi(\mathbf{x}, t)$  is defined as the signed normal distance from the solid–liquid interface, with  $\phi > 0$  in the liquid phase,  $\phi < 0$  in the solid phase, and  $\phi = 0$  on the interface  $\Gamma(t) = \{\mathbf{x} : \phi(\mathbf{x}, t) = 0\}$ . The interface is evolved by advecting  $\phi$  according to

$$\phi_t + F(\mathbf{x}, t) |\nabla \phi| = 0, \quad (18)$$

where  $F$  is a velocity field constructed as an extension of the normal interface velocity following the classical level-set formulation for Stefan problems [33].

The normal velocity of the interface is defined only on  $\Gamma(t)$  through the Stefan condition,

$$V_n(\mathbf{x}, t) = \frac{1}{\rho_s L} (k_s \nabla u_s \cdot \mathbf{n} - k_\ell \nabla u_\ell \cdot \mathbf{n}), \quad \mathbf{x} \in \Gamma(t), \quad (19)$$

where the unit normal vector is obtained from the level-set function as

$$\mathbf{n} = \frac{\nabla \phi}{|\nabla \phi|}. \quad (20)$$

Since the Stefan condition provides the interface velocity only on  $\Gamma(t)$ , the velocity field  $F$  is constructed by extending  $V_n$  off the interface along normal directions. Because  $\phi$  represents the signed distance to the interface, each collocation point  $\mathbf{x} \in \Omega$  is associated with a unique point on the interface given by the normal projection

$$\mathbf{x}_\Gamma = \mathbf{x} - \phi(\mathbf{x}, t) \mathbf{n}(\mathbf{x}, t), \quad (21)$$

which satisfies  $\mathbf{x}_\Gamma \in \Gamma(t)$ . The normal interface velocity is evaluated at the projected point  $\mathbf{x}_\Gamma$  using (19), and the resulting value is assigned to the original point  $\mathbf{x}$ , defining the extended velocity field

$$F(\mathbf{x}, t) = V_n(\mathbf{x}_\Gamma, t). \quad (22)$$

By construction,  $F$  is constant along normal rays to the interface.

The level-set evolution equation (18) is enforced in a weak sense at all collocation points through the advection loss

$$\mathcal{L}_{\text{Advection}} = \|\phi_t + F(\mathbf{x}, t) |\nabla \phi|\|^2. \quad (23)$$

Since the velocity extension relies on  $\phi$  remaining a signed-distance function, the condition  $|\nabla \phi| = 1$  is weakly enforced via the Eikonal regularization

$$\mathcal{L}_{\text{Eikonal}} = \||\nabla \phi| - 1\|^2, \quad (24)$$

which eliminates the need for explicit reinitialization.

The boundary and initial conditions are imposed weakly through the loss terms

$$\mathcal{L}_{\text{BC}} = \mathbb{E}_{\mathbf{x} \in \partial\Omega, t} \left[ \|u(\mathbf{x}, t) - u_D(\mathbf{x}, t)\|^2 + \|\nabla u(\mathbf{x}, t) \cdot \mathbf{n} - g_N(\mathbf{x}, t)\|^2 \right], \quad (25)$$

$$\mathcal{L}_{\text{IC}} = \mathbb{E}_{\mathbf{x} \in \Omega} \left[ \|u(\mathbf{x}, 0) - u_0(\mathbf{x})\|^2 + \|\phi(\mathbf{x}, 0) - \phi_0(\mathbf{x})\|^2 \right], \quad (26)$$

where  $u_D$  and  $g_N$  denote prescribed Dirichlet and Neumann boundary data, respectively, and  $u_0$  and  $\phi_0$  are the initial temperature and phase distributions.

Training points are generated as follows:

- **Collocation points:** uniformly sampled throughout the spatio-temporal domain, with additional points concentrated near the interface  $\Gamma(t)$  to enhance accuracy in regions with steep temperature gradients.
- **Boundary points:** used to impose boundary conditions through  $\mathcal{L}_{\text{BC}}$ .
- **Initial points:** used to satisfy  $\mathcal{L}_{\text{IC}}$ , defining the initial temperature distribution and initial interface location.

The training data generation method is summarized below.

**Algorithm 1:** Adaptive Training Data Generation

**Input:** Batch size  $\{N_{\text{dom}}, N_{\text{bc}}, N_{\text{ic}}\}$ , Physics Parameters  $\mathcal{P}$ , Current Model  $\mathcal{M}_{\theta}$

**Output:** Training Datasets  $\mathcal{D}_{\text{dom}}, \mathcal{D}_{\text{bc}}, \mathcal{D}_{\text{ic}}$

Extract domain size  $L$  and time range  $[t_{\text{start}}, t_{\text{end}}]$  from  $\mathcal{P}$ ;

$N_{\text{interface}} \leftarrow 0.3 \times N_{\text{dom}}$ ,  $N_{\text{uniform}} \leftarrow N_{\text{dom}} - N_{\text{interface}}$ ;

Sample set  $X_{\text{uniform}}$  of  $N_{\text{uniform}}$  points uniformly from  $\Omega \times [t_{\text{start}}, t_{\text{end}}]$ ;

Sample candidate pool  $X_{\text{pool}}$  of  $10 \times N_{\text{interface}}$  points uniformly;

Compute level-set predictions  $\hat{\phi} \leftarrow \mathcal{M}_{\phi}(X_{\text{pool}})$ ;

Select  $X_{\text{interface}} \subset X_{\text{pool}}$  with smallest  $|\hat{\phi}|$  such that  $\|X_{\text{interface}}\| = N_{\text{interface}}$ ;

$\mathcal{D}_{\text{dom}} \leftarrow X_{\text{uniform}} \cup X_{\text{interface}}$ , enable gradients;

Sample  $N_{\text{bc}}$  points  $\mathbf{x}_{\text{bc}}$  on  $\partial\Omega$  and compute exact  $T_{\text{bc}}$ ;

$\mathcal{D}_{\text{bc}} \leftarrow \{(\mathbf{x}_{\text{bc}}, t_{\text{bc}}), T_{\text{bc}}^{\text{exact}}\}$ ;

Sample  $N_{\text{ic}}$  points  $\mathbf{x}_{\text{ic}}$  in  $\Omega$  at  $t_{\text{start}}$  and compute exact  $T_0, \phi_0$ ;

$\mathcal{D}_{\text{ic}} \leftarrow \{(\mathbf{x}_{\text{ic}}, t_{\text{start}}), T_0, \phi_0\}$ ;

**return**  $\{\mathcal{D}_{\text{dom}}, \mathcal{D}_{\text{bc}}, \mathcal{D}_{\text{ic}}\}$

KANs are motivated by the Kolmogorov–Arnold representation theorem, which states that any continuous multivariate function  $f : [0, 1]^n \rightarrow \mathbb{R}$  can be written in the form

$$f(x_1, \dots, x_n) = \sum_{q=1}^{2n+1} \Phi_q \left( \sum_{p=1}^n \varphi_{q,p}(x_p) \right), \quad (27)$$

where each  $\varphi_{q,p} : [0, 1] \rightarrow \mathbb{R}$  and  $\Phi_q : \mathbb{R} \rightarrow \mathbb{R}$  are univariate continuous functions [26].

In the KAN architecture, this theorem is generalized: instead of fixed linear weights and node-wise activation functions, *each weight* connecting layer  $l$  to  $l+1$  is replaced by a learnable univariate function (parametrized by a spline) acting on the input coordinate, and then summed across inputs. Thus, a KAN layer of shape  $[m, n]$  can be viewed as a matrix of functions  $[\varphi_{ij}]$ , where

$$\Phi(x) = \begin{pmatrix} \varphi_{11}(x_1) + \dots + \varphi_{1m}(x_m) \\ \vdots \\ \varphi_{n1}(x_1) + \dots + \varphi_{nm}(x_m) \end{pmatrix}. \quad (28)$$

KANs stack such layers, allowing compositions of these “univariate-edge, sum-node” layers to build expressive models. Because the univariate functions (splines) are learned, KANs can adaptively shape nonlinearity per edge, rather than relying on a fixed activation per neuron. Empirically, this leads to more parameter-efficient representations compared to standard MLPs for tasks including function approximation and PDE solving [26].

The training procedure for the KAN framework is structurally similar in both the one-dimensional and two-dimensional Stefan problems. We employ the AdamW optimizer with weight decay regularization and a learning rate scheduler to adaptively reduce the step size when the loss plateaus.

During optimization, gradient clipping is applied to avoid exploding gradients, and resampling of collocation points is performed iteratively to improve resolution near the moving interface. This adaptive resampling ensures that steep gradients at the solid–liquid boundary are accurately captured as training progresses. The overall training iteration for the n-dimensional Stefan problem is summarized below.

**Algorithm 2:** Training Iteration for the nD Stefan KAN

```

for  $epoch = 1, 2, \dots, N$  do
    Sample collocation points  $(\mathbf{x}_f, t_f)$ , boundary points  $(\mathbf{x}_b, t_b)$ , and initial points
     $(\mathbf{x}_0, t_0)$ ;
    Compute network predictions  $u_1(\mathbf{x}, t), u_2(\mathbf{x}, t), \Gamma(t)$ ;
    Evaluate PDE residuals  $\mathcal{L}_{PDE,l}, \mathcal{L}_{PDE,s}$ , interface loss  $\mathcal{L}_{Stefan}$ ,
    continuity losses  $\mathcal{L}_{Cont,u_1}, \mathcal{L}_{Cont,u_2}$ , boundary loss  $\mathcal{L}_{BC}$ , and initial loss  $\mathcal{L}_{IC}$ ;
    Form total loss  $\mathcal{L} = \sum_i w_i \mathcal{L}_i$ ;
    Compute gradients  $\nabla_{\theta} \mathcal{L}$  and apply gradient clipping;
    Update parameters  $\theta \leftarrow \theta - \eta \nabla_{\theta} \mathcal{L}$  (AdamW);
end

```

### 3 Results

#### 3.1 1D Stefan Problem: Temperature and Interface Evolution

We first validate the proposed KAN framework on the one-dimensional two-phase Stefan problem. The spatial domain is the unit interval  $\Omega = [0, 1]$ , initially divided into solid and liquid regions separated by an interface located at  $x = s_0$ .

The governing conditions are: Initial condition (IC):  $u(x, 0) = T_1$  for  $x < s_0$  and  $T_2$  for  $x \geq s_0$ , where  $T_1 < T_m < T_2$ ; Boundary conditions (BC):  $u(0, t) = T_1$ ,  $u(1, t) = T_{exact}(1, t)$ , where  $T_{exact}(x, t)$  denotes the analytical solution of the semi-infinite Stefan problem evaluated at the right boundary.

For this problem, three separate KAN subnetworks are employed: the solid-phase ( $u_s(x, t)$ ) and liquid-phase ( $u_l(x, t)$ ) temperature networks, both with a  $[2, 4, 4, 1]$  architecture, and the interface position network  $s(t)$ , which has a  $[1, 2, 2, 1]$  architecture.

This configuration was selected based on empirical evaluation and was found to provide adequate representational capacity for capturing the temperature evolution and interface motion in one dimension.

Figure 1 shows the predicted temperature profiles in both phases at different time instances, along with the evolution of the moving interface compared to the analytical solution. The results demonstrate that the network accurately captures both the smooth temperature fields and the sharp interface dynamics, confirming the effectiveness of the proposed KAN-based formulation for the 1D Stefan problem.

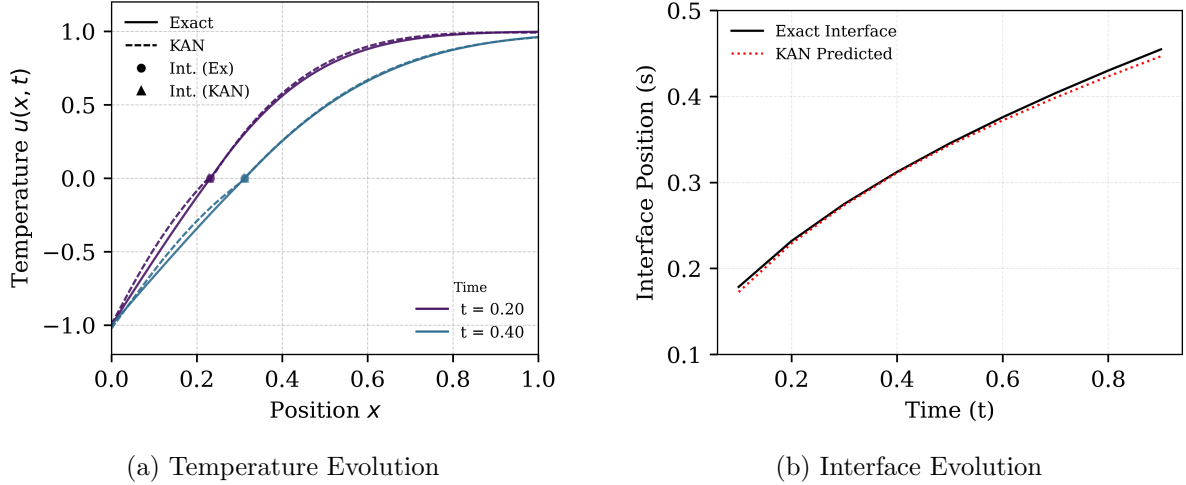


Figure 1: KAN vs. exact solution: (a) temperature, (b) interface.

Table 1: Error metrics for temperature and interface predictions at different numbers of collocation points.

$n_{\text{coll}}$	Temperature				Interface			
	MAE	MSE	RMS	$R^2$	MAE	MSE	RMS	$R^2$
500	0.0432	0.00310	0.0556	0.9913	0.0183	0.00034	0.0183	0.9670
1000	0.0278	0.00170	0.0413	0.9949	0.0084	0.00009	0.0093	0.9878
2000	0.0272	0.00153	0.0391	0.9957	0.0067	0.00005	0.0072	0.9949
4000	0.0229	0.00122	0.0349	0.9966	0.0045	0.00003	0.0054	0.9971

In our experiments, a five-layer MLP with approximately 100 neurons per layer is required for each subnetwork  $(u_s, u_\ell, s)$ , resulting in roughly  $1.2 \times 10^5$  trainable parameters, whereas the corresponding KAN-based formulation uses only 640 parameters.

### 3.2 2D Stefan Problem: Temperature and Interface Evolution

We now consider a two-dimensional Stefan problem with a circular (Frank-type) interface in order to assess the convergence and robustness of the proposed KAN framework under curved phase boundaries.

The computational domain is defined as  $\Omega = [-5, 5] \times [-5, 5]$ , containing an initially circular solid region centered at the origin with radius  $R_0 = 1.56$ . This setup corresponds to a radially symmetric Stefan problem embedded in a sufficiently large finite domain to approximate far-field conditions.

Initially, the system consists of an inner solid region ( $\|\mathbf{x}\| \leq R_0$ ) at the melting temperature  $T_m$  and an exterior subcooled liquid at  $T_\infty$ . Boundary conditions are imposed such that the temperature approaches  $T_m$  in the far field, enforced on  $\partial\Omega$  via the analytical Stefan solution, while the symmetry at the origin is satisfied by fixing  $u(0, t) = T_m$ .

Three separate KAN subnetworks were employed for this problem as well: the solid-phase ( $u_s(\mathbf{x}, t)$ ) and liquid-phase ( $u_\ell(\mathbf{x}, t)$ ) temperature networks, both with a  $[3, 8, 8, 1]$  architecture, and the level set network  $\phi(\mathbf{x}, t)$ , which also has a  $[3, 8, 8, 1]$  architecture.

Figure 2 shows the predicted temperature fields in both phases at  $t = 1.5$  compared to the analytical solution.

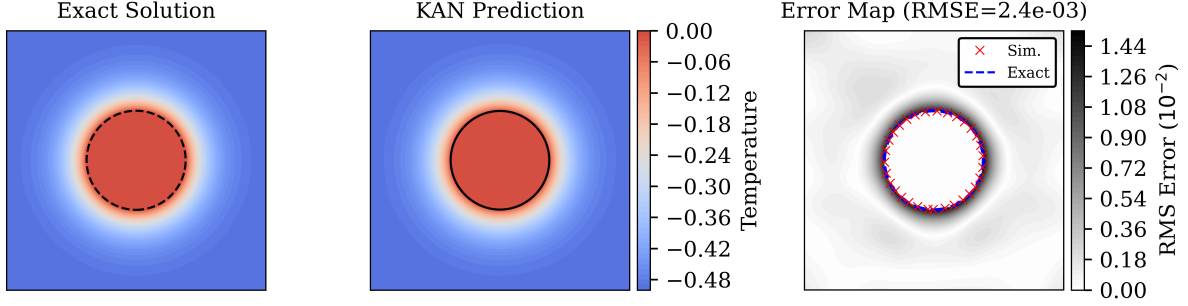


Figure 2: Evolution of the temperature field and error distribution for  $n_{coll} = 8000$  at  $t = 1.5$ .

The quantitative accuracy of the KAN framework is further analyzed in Figure 3. The temperature profiles along the symmetry axis  $y = 0$ , shown in Figure 3a, align closely with the exact solution at  $t = 1.0$  and  $t = 2.0$ . The model correctly captures the expanding isothermal solid core ( $u = 0$ ) and the smooth thermal decay in the liquid region, resolving the sharp phase boundary without significant oscillations. Furthermore, the interface dynamics presented in Figure 3b verify that the predicted radius  $R(t)$  tracks the analytical interface  $R(t) = R_0\sqrt{t}$  with high precision. This confirms that the physics-informed loss functions successfully enforce the Stefan condition governing the interface velocity.

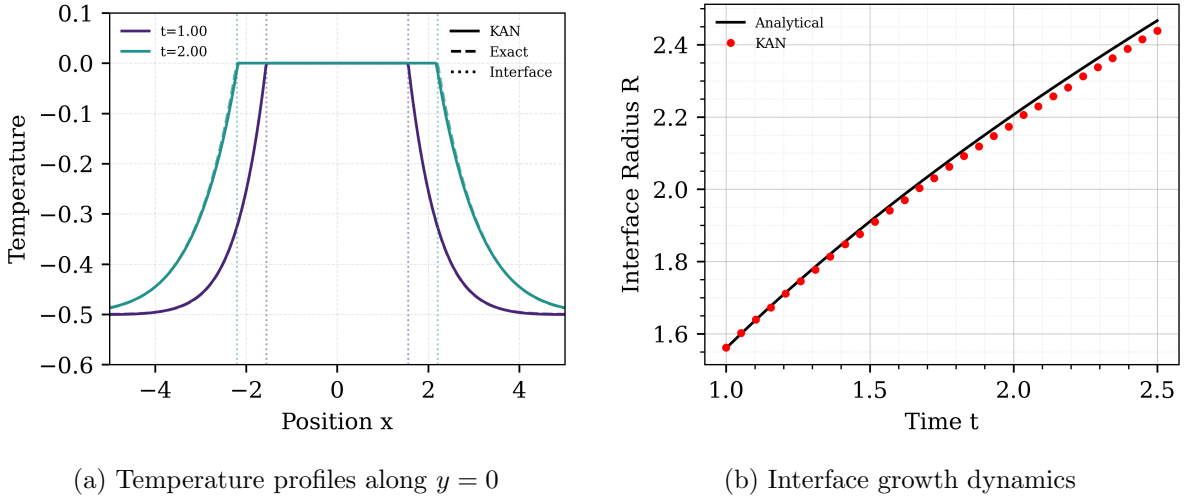


Figure 3: KAN vs. exact solution: (a) temperature, (b) interface.

We investigate the impact of collocation density by comparing models trained with varying numbers of collocation points, using space–time pointwise error metrics (MAE, MSE, and  $R^2$ ) computed against the analytical solution (signed distance function for  $\phi$ ).

Table 2: Error metrics for temperature and level set predictions for models trained with different numbers of collocation points.

$n_{\text{coll}}$	Temperature			Level Set		
	MAE	MSE	$R^2$	MAE	MSE	$R^2$
500	$2.77 \times 10^{-3}$	$3.40 \times 10^{-5}$	0.9990	$3.73 \times 10^{-2}$	$1.68 \times 10^{-3}$	0.9992
1000	$2.43 \times 10^{-3}$	$2.54 \times 10^{-5}$	0.9992	$2.90 \times 10^{-2}$	$1.04 \times 10^{-3}$	0.9995
2000	$2.13 \times 10^{-3}$	$2.08 \times 10^{-5}$	0.9994	$2.74 \times 10^{-2}$	$9.49 \times 10^{-4}$	0.9996
4000	$1.79 \times 10^{-3}$	$1.37 \times 10^{-5}$	0.9996	$2.31 \times 10^{-2}$	$6.40 \times 10^{-4}$	0.9997
8000	$1.59 \times 10^{-3}$	$1.15 \times 10^{-5}$	0.9997	$1.93 \times 10^{-2}$	$4.82 \times 10^{-4}$	0.9998
16000	$1.59 \times 10^{-3}$	$1.18 \times 10^{-5}$	0.9996	$1.99 \times 10^{-2}$	$5.09 \times 10^{-4}$	0.9998

We observe diminishing returns beyond  $n_{\text{coll}} = 8000$ , indicating that the learned solution has effectively converged with respect to collocation density.

## 4 Conclusion

A key motivation for employing Kolmogorov–Arnold Networks (KANs) in the present work is their ability to represent nonlinear mappings with significantly fewer trainable parameters than conventional multilayer perceptrons (MLPs). KANs construct multivariate functions through compositions of adaptive univariate functions, which has been shown to improve parameter efficiency and reduce redundancy compared to standard fully connected architectures. While KANs have been used for solving PDEs, the present work specifically demonstrates their relevance and superiority in handling moving boundary problems, with interface jump conditions. This overcomes the existing limitation on employing measurement data. Further, we show that the shallow networks with two hidden layers and tens of learnable parameters are sufficient, even without using measurement data, in contrast to physics-informed MLP-based formulations involving nearly a million trainable parameters.

## References

- [1] Jonathan A. Dantzig and Michel Rappaz. *Solidification*. EPFL Press, Lausanne, 2nd edition, 2016.
- [2] Shubham Chandra, Jayaraj Radhakrishnan, Sheng Huang, Siyuan Wei, and Upadrashta Ramamurty. Solidification in metal additive manufacturing: challenges, solutions, and opportunities. *Progress in Materials Science*, 148:101361, 2025.
- [3] Ashwin J. Shahani and Amy J. Clarke. Processing metallic materials far from equilibrium. *MRS Bulletin*, 45(11):906–909, 2020.
- [4] Usman Masood, Mahmoud Haggag, Ahmed Hassan, and Mohammad Laghari. A review of phase change materials as a heat storage medium for cooling applications in the built environment. *Buildings*, 13(7), 2023.
- [5] Shang Gao, Yaxiong Yang, Aleksandra S. Falchevskaya, Vladimir V. Vinogradov, Bo Yuan, Jing Liu, and Xuyang Sun. Phase transition liquid metal enabled emerging biomedical technologies and applications. *Advanced Science*, 11(37):2306692, 2024.
- [6] Paul CW Davies, Lloyd Demetrius, and Jack A. Tuszynski. Cancer as a dynamical phase transition. *Theoretical Biology and Medical Modelling*, 8(1):30, August 2011.

- [7] Ranpeng Li, Juliane Dannberg, Rene Gassmöller, Carolina Lithgow-Bertelloni, and Lars Stixrude. How phase transitions impact changes in mantle convection style throughout earth's history: From stalled plumes to surface dynamics. *Geochemistry, Geophysics, Geosystems*, 26(2):e2024GC011600, 2025. e2024GC011600 2024GC011600.
- [8] Stephen H. Davis. *Theory of Solidification*. Cambridge Monographs on Mechanics. Cambridge University Press, Cambridge, 2001.
- [9] Yohei Sato and Bojan Ničeno. A sharp-interface phase change model for a mass-conservative interface tracking method. *Journal of Computational Physics*, 249:127–161, 2013.
- [10] Nicolò Scapin, Pedro Costa, and Luca Brandt. A volume-of-fluid method for interface-resolved simulations of phase-changing two-fluid flows. *Journal of Computational Physics*, 407:109251, 2020.
- [11] Xi Liu, Zhenhua Chai, Chengjie Zhan, Baochang Shi, and Wenhuan Zhang. A diffuse-domain phase-field lattice boltzmann method for two-phase flows in complex geometries. *Multiscale Modeling & Simulation*, 20(4):1411–1436, 2022.
- [12] J. C. Ramirez, C. Beckermann, A. Karma, and H.-J. Diepers. Phase-field modeling of binary alloy solidification with coupled heat and solute diffusion. *Phys. Rev. E*, 69:051607, May 2004.
- [13] Satoshi Ii, Kazuyasu Sugiyama, Shintaro Takeuchi, Shu Takagi, Yoichiro Matsumoto, and Feng Xiao. An interface capturing method with a continuous function: The thinc method with multi-dimensional reconstruction. *Journal of Computational Physics*, 231(5):2328–2358, 2012.
- [14] N.S. Asaithambi. A galerkin method for stefan problems. *Applied Mathematics and Computation*, 52(2):239–250, 1992.
- [15] Xiangwei Dong, Guannan Hao, and Ran Yu. Two-dimensional smoothed particle hydrodynamics (sph) simulation of multiphase melting flows and associated interface behavior. *Engineering Applications of Computational Fluid Mechanics*, 16(1):588–629, 2022.
- [16] Frederic Gibou, Ronald P. Fedkiw, Li-Tien Cheng, and Myungjoo Kang. A second-order-accurate symmetric discretization of the poisson equation on irregular domains. *Journal of Computational Physics*, 176(1):205–227, 2002.
- [17] M. Raissi, P. Perdikaris, and G. E. Karniadakis. Physics-informed neural networks: A deep learning framework for solving forward and inverse problems involving nonlinear partial differential equations. *Journal of Computational Physics*, 378:686–707, 2019.
- [18] Shengze Cai, Zhicheng Wang, Sifan Wang, Paris Perdikaris, and George Em Karniadakis. Physics-Informed Neural Networks for Heat Transfer Problems. *Journal of Heat Transfer*, 143(060801), April 2021.
- [19] Jeremy Yu, Lu Lu, Xuhui Meng, and George Em Karniadakis. Gradient-enhanced physics-informed neural networks for forward and inverse pde problems. *Computer Methods in Applied Mechanics and Engineering*, 393:114823, 2022.
- [20] Sanjeet Patra, Manish Agrawal, Prasenjit Rath, and Anirban Bhattacharya. Physics informed neural network-based framework for two-dimensional phase change problems. *Computer Physics Communications*, 317:109854, 2025.

- [21] Yuan Cao, Zhiying Fang, Yue Wu, Ding-Xuan Zhou, and Quanquan Gu. Towards understanding the spectral bias of deep learning, 2020.
- [22] Nasim Rahaman, Aristide Baratin, Devansh Arpit, Felix Draxler, Min Lin, Fred A. Hamprecht, Yoshua Bengio, and Aaron Courville. On the spectral bias of neural networks, 2019.
- [23] Salvatore Cuomo, Vincenzo Schiano Di Cola, Fabio Giampaolo, Gianluigi Rozza, Maziar Raissi, and Francesco Piccialli. Scientific Machine Learning Through Physics-Informed Neural Networks: Where we are and What's Next. *Journal of Scientific Computing*, 92(3):88, July 2022.
- [24] Sokratis J. Anagnostopoulos, Juan Diego Toscano, Nikolaos Stergiopoulos, and George Em Karniadakis. Learning in pinns: Phase transition, diffusion equilibrium, and generalization. *Neural Networks*, 193:107983, 2026.
- [25] Mathieu Mullins, Hamza Kamil, Adil Fahsi, and Azzeddine Soulaïmani. Physics-informed neural networks for solving moving interface flow problems using the level set approach. *Physics of Fluids*, 37(10):107124, 10 2025.
- [26] Ziming Liu, Yixuan Wang, Sachin Vaidya, Yifan Zhang, Yao Zhang, Guoqiang Lin, and George Em Karniadakis. Kan: Kolmogorov-Arnold Networks. April 2024. arXiv:2404.19756 [cs, stat].
- [27] Andrey Nikolaevich Kolmogorov. On the representation of continuous functions of several variables by superpositions of continuous functions of a smaller number of variables. *Doklady Akademii Nauk SSSR*, 108(2):179–182, 1956.
- [28] Andrey Nikolaevich Kolmogorov. On the representation of continuous functions of many variables by superposition of continuous functions of one variable and addition. *Doklady Akademii Nauk SSSR*, 114(5):953–956, 1957.
- [29] Yixuan Wang, Jonathan W. Siegel, Ziming Liu, and Thomas Y. Hou. On the expressiveness and spectral bias of kans, 2025.
- [30] S. Osher and J. A. Sethian. Fronts propagating with curvature-dependent speed: Algorithms based on hamilton–jacobi formulations. *Journal of Computational Physics*, 79(1):12–49, 1988.
- [31] J. Crank. *Free and Moving Boundary Problems*. Oxford University Press, Oxford, 1984.
- [32] L. I. Rubinstein. *The Stefan Problem*, volume 27 of *Translations of Mathematical Monographs*. American Mathematical Society, Providence, RI, 1971.
- [33] Yung-Tae Kim, Nigel Goldenfeld, and Jonathan Dantzig. Computation of dendritic microstructures using a level set method. *Phys. Rev. E*, 62:2471–2474, Aug 2000.